AAS 16-221

LDSD POST2 MODELING ENHANCEMENTS IN SUPPORT OF SFDT-2 FLIGHT OPERATIONS

Joseph White*, Angela L. Bowes†, Soumyo Dutta‡, Mark C. Ivanov§, Eric M. Queen**

Program to Optimize Simulated Trajectories II (POST2) was utilized to develop trajectory simulations characterizing all flight phases from drop to splashdown for the Low-Density Supersonic Decelerator (LDSD) project's first and second Supersonic Flight Dynamics Tests (SFDT-1 and SFDT-2) which took place June 28, 2014 and June 8, 2015, respectively. This paper describes the modeling improvements incorporated into the LDSD POST2 simulations since SFDT-1 and presents how these modeling updates affected the predicted SFDT-2 performance and sensitivity to the mission design. The POST2 simulation flight dynamics support during the SFDT-2 launch, operations, and recovery is also provided.

INTRODUCTION

The Supersonic Flight Dynamics Test (SFDT) vehicle was developed to advance and test technologies of NASA's Low Density Supersonic Decelerator (LDSD) technology demonstration mission[1, 2]. Test flights were conducted in June of 2014 (SFDT-1) and June of 2015 (SFDT-2), which provided substantial amounts of data to help improve and further develop deceleration technologies. These data have been used in extensive post-flight reconstruction efforts for both flights.

Independent Program to Optimize Simulated Trajectories II (POST2)[3] six degree-of-freedom (6DOF) and multi-body 6DOF trajectory simulations characterizing all SFDT flight phases were developed at NASA's Langley Research Center (LaRC) as part of a simulation suite utilized by the LDSD Project in support of SFDT-1 and SFDT-2.[4] The simulations model all flight phases and events of the test, including balloon drop, spin up, main motor burn, spin down, inflation of the Supersonic Inflatable Aerodynamic Decelerator (SIAD), ballute mortar fire and inflation, parachute extraction and inflation, and splashdown. The multi-body capability of POST2 allows for the test vehicle (TV), ballute parachute deployment device (PDD), and supersonic ring sail parachute (SSRS) to be modeled as separate, but coupled bodies throughout all phases and events. These simulations are used to perform various flight dynamics analyses as well as Monte Carlo analyses with various parameter dispersions to provide probabilistic performance envelopes and sensitivities.

* Senior Project Engineer, Analytical Mechanics Associates, Inc, 21 Enterprise Parkway Suite 300, Hampton, VA 23666-6413, joseph.white@nasa.gov.
† Aerospace Engineer, NASA Langley Research Center, MS 489, Hampton, VA 23681-2199, angela.bowes@nasa.gov
‡ Aerospace Engineer, NASA Langley Research Center, MS 489, Hampton, VA 23681-2199, soumyo.dutta@nasa.gov.
§ Senior Guidance and Controls Engineer, Jet Propulsion Laboratory, 4800 Oak Grove Drive M/S 321-220, Pasadena, CA, mark.c.ivanov@jpl.nasa.gov.
** Aerospace Engineer, NASA Langley Research Center, MS 489, Hampton, VA 23681-2199, eric.m.queen@nasa.gov.

The SFDT-1 post-flight reconstruction analyses provided various insights into the simulation models and their predictive capabilities. Several models were identified which could be improved upon to aid in analyses for the following SFDT-2 flight. These models include: thrust modeling and dispersions for the main motor; test vehicle aerodynamic modeling; ballute free flying aerodynamics and tracking; supersonic ring sail aerodynamic modeling; day-of-flight atmospheric dispersion modeling; and flight software dynamic event triggering. Background information on these models, what updates were made, and their impact on SFDT-2 analyses and operations are detailed in this document.

OVERVIEW

Many dynamic events in the SFDT flights affect the performance of the vehicle and analyses performed. **Figure 1** gives a graphical representation of the primary events to be described.

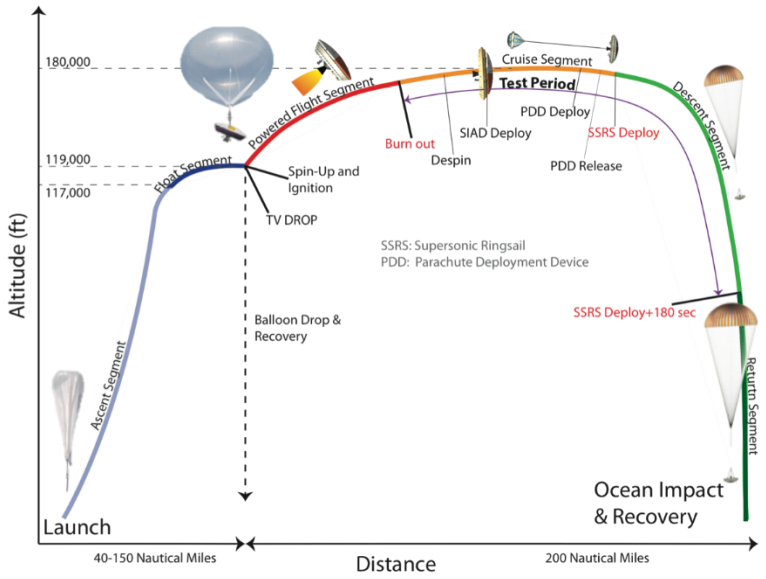

Figure 1: SFDT-2 flight concept of operations

The simulations begin with the TV drop from the ascent balloon. The spin motors then fire to stabilize the TV during powered flight, after which the Star 48 fires. After burnout has been sensed, additional spin motors de-spin the vehicle ending the powered flight phase. Once de-spun, the SIAD inflates based on a velocity trigger, beginning the test period of flight. At the end of the test period, the PDD is deployed via mortar fire, which is based on an additional velocity trigger. This then extracts the SSRS pack from the TV and begins the parachute inflation process and descent segment of flight. Once the vehicle splashes down, the recovery vessels collect all possible expended flight hardware: balloon, TV with SSRS, and PDD.

The events described above all have significant effects on the TV dynamics which impacts the probability of successful downstream events. In particular, the powered flight sets up much of the dynamics that will play a heavy role in the success of all following events. The Monte Carlo analyses help provide insight into whether the dynamic behavior and vehicle performance will meet mission requirements.

These Monte Carlo analyses take into account uncertainties on model parameters and applies them in random combinations over a specified number of runs. Dispersions are sometimes also applied individually or in groups to determine the individual or group effects on results. For

example, a dispersion only in the axial center of mass of the TV might be examined for its effect on attitude oscillation. Or, alternatively, all atmospheric dispersions could be applied as a group to determine their effect on parachute deployment conditions. The variety and versatility of Monte Carlo analyses performed provides a detailed picture of the expected test performance. Some performance parameters of particular interest with respect to the modeling updates to be described are the angle of attack and rate after powered flight, camera visibility of the PDD and SSRS deployment and inflation events, and splashdown location and footprint of each vehicle for recovery efforts.

MODELING UPDATES

After the SFDT-1 post-flight reconstruction analysis[5,6], several models in POST2 were identified where improvements or enhancements could be made for SFDT-2. For example, the SFDT-1 flight demonstrated significant lofting as compared to pre-flight predictions. During the reconstruction process, the models that showed the largest impact on lofting were the atmosphere, Star 48 thrust, and aerodynamic models. Using reconstructed atmosphere and thrust profiles, along with an adjustment to pitch and yaw coefficients at low Mach values, accounted for nearly all of the lofting discrepancy. There have also been notable updates in the TV aerodynamics, PDD aerodynamics and event triggering, which all improved capability and accuracy leading up to the SFDT-2 flight.

These model updates were brought into the LDSD code for use in SFDT-2 pre-flight analyses and operations. The individual model updates are described in the sections that follow.

Thrust Modeling and Dispersions for Main Motor

The main motor on the SFDT vehicles in both flown tests is a Star 48 motor. The long burn time of the motor early in the trajectory causes it to have a significant impact on downstream events. In SFDT-1, the reconstructed thrust profile was seen as a top three contributor to accounting for lofting differences in pre-flight and as-flown trajectories. Therefore, understanding how to model the thrust and its uncertainties most accurately becomes critical.

For SFDT-1 analyses and operation, dispersions were applied to the magnitude of the nominal thrust profile, maintaining total impulse over the burn to within 0.5% 3-sigma. This allowed for scaling in magnitude and time of the thrust profile as depicted in **Figure 2**. The post-flight reconstruction work for SFDT-1[7, 8] showed that the flown thrust profile not only varied in magnitude and time, but also in its pro/regressive nature (slope or shape) as can be seen in **Figure 3**. This variation from nominal was not unexpected by ATK given that the motor had propellant off-loaded to meet the needs of the LDSD program.

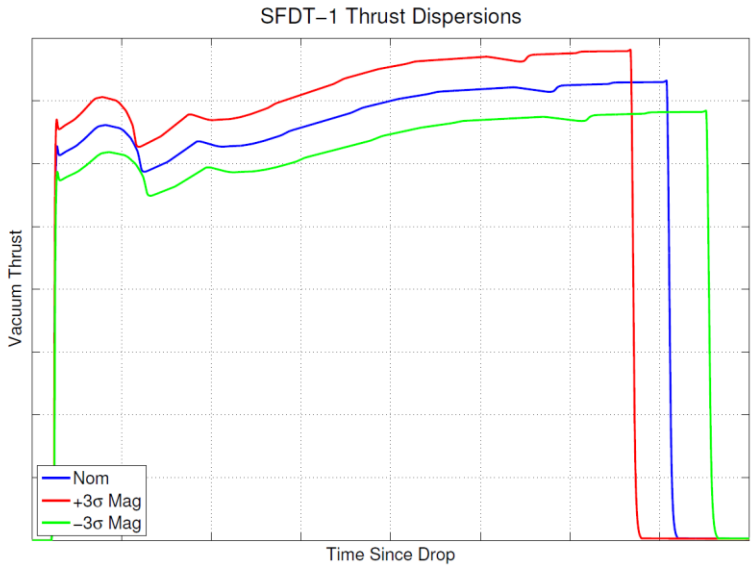

Figure 2: Thrust profile and dispersion model for SFDT-1, limited to magnitude only

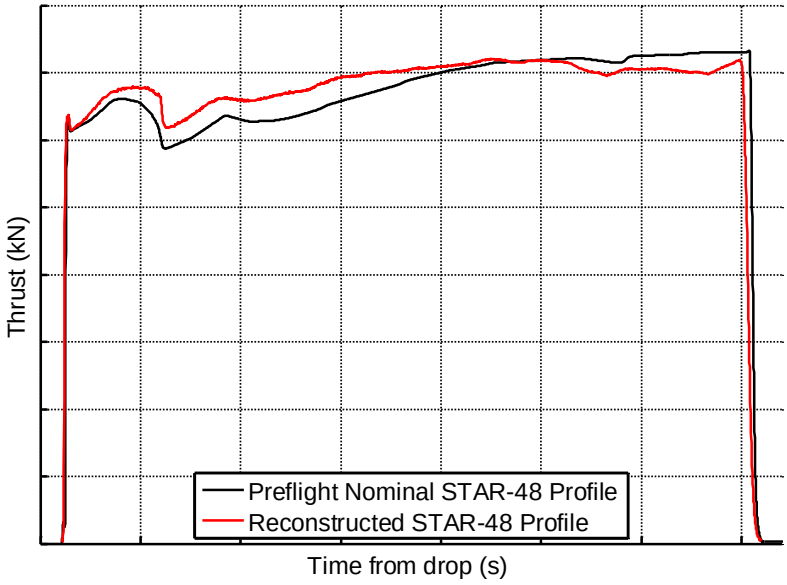

Figure 3: SFDT-1 Predicted and reconstructed thrust profiles.

As can be seen, the reconstructed thrust profile flown in SFDT-1 was not a possible scenario in any of the simulation runs performed pre-flight using the dispersion model described above since it did not allow any variations in shape. Because propellant was also off-loaded for the Star 48 motor being used on SFDT-2 the more regressive profile is still a plausible scenario. Due to these various facts, it was determined that a more representative and conservative method of dispersing the thrust would be needed for SFDT-2 analyses.

In order to capture not only thrust magnitude and impulse dispersions, but the pro/regressive characteristics of the profile, a new dispersion model was derived. A linear function $K(t)$ is used to scale the thrust magnitude:

$$K(t) = at + b \quad (1)$$

A function $\Gamma(t_b)$ is defined as:

$$\Gamma(t_b) = \int_0^{t_b} \int_0^t T(\tau) d\tau \, dt \quad (2)$$

Where $T(\tau)$ is the nominal thrust profile and t_b is the nominal burn time. It can be shown that as long as a and b satisfy:

$$b = \left[\frac{\Gamma(t_b)}{I(t_b)} - t_b\right] a + 1 \quad (3)$$

Where $I(t_b)$is the nominal total impulse:

$$I(t_b) = \int_0^{t_b} T(\tau) d\tau \quad (4)$$

Then $T(t)K(t)$ will preserve total impulse. Assuming that this shape dispersion does not alter I_{sp}, the same function $K(t)$ can be applied to the mass flow rate so that thrust remains correlated with mass loss. For time-scaled thrust profiles:

$$\Gamma(t_b') = \left(\frac{t_b'}{t_b}\right)^2 \Gamma(t_b) \quad (5)$$

And

$$b' = \left(\frac{t_b'}{t_b}\right)\left[\frac{\Gamma(t_b)}{I(t_b)} - t_b\right] a + 1 \quad (6)$$

$T(\tau)$ is not actually available in simulation as a continuous function of time. Instead, we have:

$$T = T(i) \quad (7)$$

Where each $T(i)$ is separated from the next and previous by a nominal time Δt.

Burn time is dispersed by stretching or compressing Δt. The integral is approximated by:

$$\int_0^{t_b} T(\tau) d\tau = \sum T(i) \cdot \Delta t \quad (8)$$

If $t_b$is replaced by t_b' and

$$\Delta t' = \left(\frac{t'_b}{t_b}\right) \Delta t \quad (9)$$

The following can be shown:

$$\int_0^{t_b'} T(\tau) d\tau = \sum T(i) \cdot \left(\frac{t'_b}{t_b}\right) \Delta t = \left(\frac{t'_b}{t_b}\right) \sum T(i) \cdot \Delta t = \left(\frac{t'_b}{t_b}\right) \int_0^{t_b} T(\tau) d\tau \quad (10)$$

And similarly,

$$\Gamma(t_b') = \sum T(i) \cdot \left(\frac{t'_b}{t_b}\right)^2 \Delta t^2 = \left(\frac{t'_b}{t_b}\right)^2 \sum T(i) \cdot \Delta t^2 = \left(\frac{t_b'}{t_b}\right)^2 \Gamma(t_b) \quad (11)$$

Note that even if $T(\tau)$ were available as a continuous function of time, the above argument would still hold for sufficiently small Δt.

Finally, in order to disperse mass flow and preserve total mass, a similar linear function is created:

$$Q(t) = at + b \quad (12)$$

And:

$$\Omega(t_b) = \int_0^{t_b} \int_0^t \dot{m}(\tau) d\tau \, dt \quad (13)$$

Where $\dot{m}(\tau)$ is the nominal mass flow rate and t_b is the nominal burn time. It can be shown that as long as a and b satisfy:

$$b = \left[\frac{\Omega(t_b)}{M(t_b)} - t_b\right] a + 1 \quad (14)$$

Where $M(t_b)$is the nominal fuel used:

$$M(t_b) = \int_0^{t_b} \dot{m}(\tau) d\tau \quad (15)$$

Then $M(t)Q(t)$ will preserve fuel consumption. For time-scaled profiles:

$$\Omega(t_b') = \left(\frac{t_b'}{t_b}\right)^2 \Omega(t_b) \quad (16)$$

And

$$b' = \left(\frac{t_b'}{t_b}\right)\left[\frac{\Omega(t_b)}{M(t_b)} - t_b\right] a + 1 \quad (17)$$

The end result of the updated thrust modeling is a dispersion set that accounts not only for magnitude and time scale differences in the thrust profile, but also more progressive and regressive profile shape changes. **Figure 4** illustrates a range of dispersed thrust profiles using the updated method. Solid lines represent the nominal and magnitude only dispersion of the thrust (limit of SFDT-1 model), dashed represent the additional progressive shape dispersion, and dash-dot lines represent the additional regressive shape dispersion. Note that the impulse preservation is evident through time scaling of the dispersed thrust profiles (i.e., lower thrust magnitude burns longer). This additional capability allows for the simulations to capture the behavior that was seen in the SFDT-1 post-flight reconstruction work, but not modeled in pre-flight analysis.

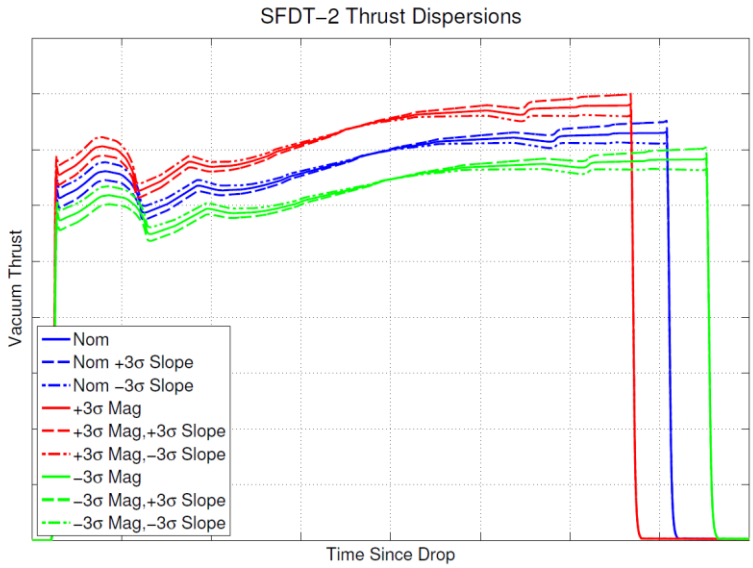

Figure 4: Thrust profile and dispersions for SFDT-2, allowing for magnitude and progressive/regressive shape adjustments

Test Vehicle Aerodynamic Modeling

Much like the significance of the thrust modeling, the aerodynamic model for the TV, especially during powered flight at low Mach, plays a significant role in downstream event conditions and overall mission performance. This was evident in SFDT-1 reconstruction as a change in TV powered flight aerodynamics was shown to be a top three contributor to the lofting discrepancy seen between pre-flight and as flown trajectories [5]. Previous modeling techniques did not capture certain aspects of the SFDT-1 trajectory as part of the Monte Carlo analyses. Updates have been made to the TV aerodynamics for SFDT-2 to remedy that situation.

There were several minor changes to the aerodynamic model including a capability to account for spin motor plume interactions, additional CFD data, and other improvements[7]. Of more significant effect, however, was an update to correlate the pitch and yaw moment coefficient dispersion multipliers and adjust their effect at low Mach. Correlating the pitch and yaw moment dispersions to be the same for a given run resolved a disparity between the two that would not be exhibited in flight. Additionally, the reduction of pitch and yaw moment coefficients at low Mach was shown to significantly increase lofting of the vehicle, which was seen in SFDT-1, but not captured in pre-flight analyses. The effect of these adjustments was found during the SFDT-1 reconstruction efforts, then validated and implemented through use of CFD data in preparation for SFDT-2. The updates allow for improved aerodynamic modeling, especially at low Mach numbers which have a strong effect on downstream events.

Ballute Free Flying Aerodynamics and Tracking

The ballute (PDD) is used to stabilize the TV prior to parachute deploy and provides the extraction force for the deployment event itself. From mortar fire, which deploys the PDD, until bag strip of the parachute, the PDD is tethered to the TV through its suspension and bridle lines prior to parachute deploy and additionally through the parachute suspension and bridle lines during parachute deploy. While tethered, the wake effects of the TV on the PDD are modeled and heavily affect the aerodynamic response of the vehicle which in turn affects the parachute deployment event conditions. Once bag strip occurs, the PDD becomes a free flying vehicle, no longer tethered to

the TV in any way. No free flying aerodynamics for the PDD were modeled with SFDT-1 and the vehicle was disabled in the multi-body simulation after bag strip.

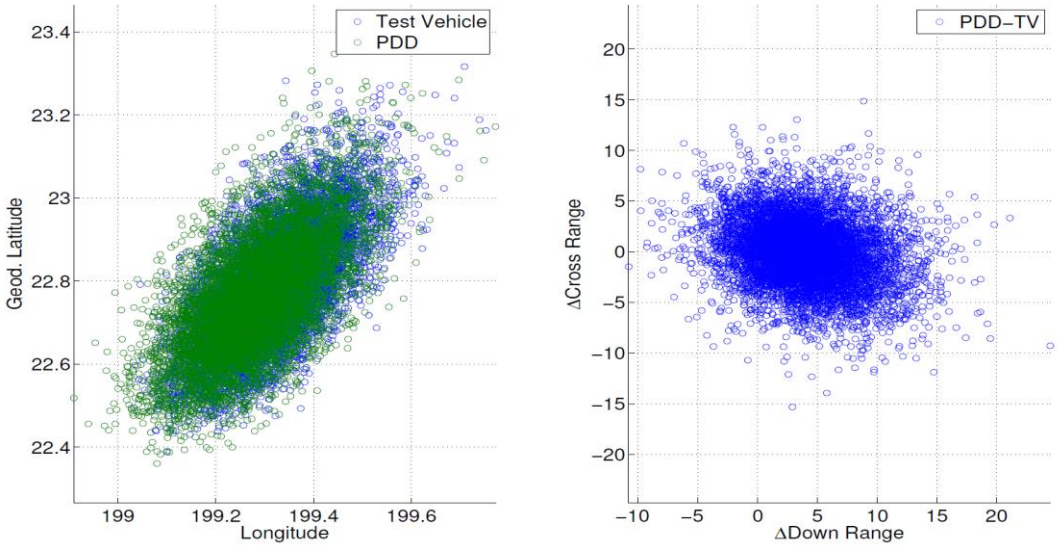

Figure 5: Sample splashdown of SFDT test vehicle and PDD (left) and relative crossrange/downrange distance from SFDT test vehicle to PDD at splashdown (right).

For SFDT-2, there was a much stronger desire to ensure recovery of all bodies from the test. To that end, for the PDD recovery, free flying aerodynamic modeling capability was included in POST2 for SFDT-2 analyses. Once bag strip of the parachute occurs, the PDD aerodynamic modeling is switched to a conservative, drag only model which is maintained for the remainder of the trajectory. Dispersions were added to this additional aerodynamic model and the PDD tracked to splashdown. Sample splashdown footprint results are shown in **Figure 5**, similar to actual day-of-flight data used in the recovery efforts of the PDD article in SFDT2 operations. Both the PDD absolute splashdown location and the splashdown location relative to the TV are obtained for analysis and recovery purposes. The results provided during operations were delivered to the recovery vessels and helped ensure successful recovery of the PDD article.

Supersonic Ring Sail Aerodynamic Modeling

Unlike the Disk-Sail shape used for SFDT-1, SFDT-2 utilized a re-designed, 30.4 m Ringsail parachute during the supersonic flight test in Kauai. Similar to the implementation for SFDT-1[Error! Bookmark not defined.], the POST2 flight dynamics simulation had two different modes – one with a drag-only model of the parachute and another that utilized a complete static aerodynamic model of the parachute and treated the parachute as a separate vehicle.

Since there was a new parachute, the drag-only and static aerodynamic data sets were both updated based on new wind tunnel tests that were done at NASA Langley Research Center in late 2014[8]. The drag-only aerodynamic model, which ignores the trimming dynamics of the parachute, was similar in form to the SFDT-1 Disk-Sail data with the exception that the new Ringsail drag coefficients were expectedly higher. However, the static aerodynamic data revealed a noticeable difference in the behavior of the new parachute at high angle of attacks when compared to the SFDT-1 Disk-Sail. As seen in **Figure 6**, at high angles of attack, the SFDT-2 parachute's nominal normal force coefficient (C_N) and pitching moment coefficient (C_m) are neutrally stable, as opposed

to the strong restorative force and moments seen in the nominal profile of the SFDT-1 parachute that was modeled in the simulation.

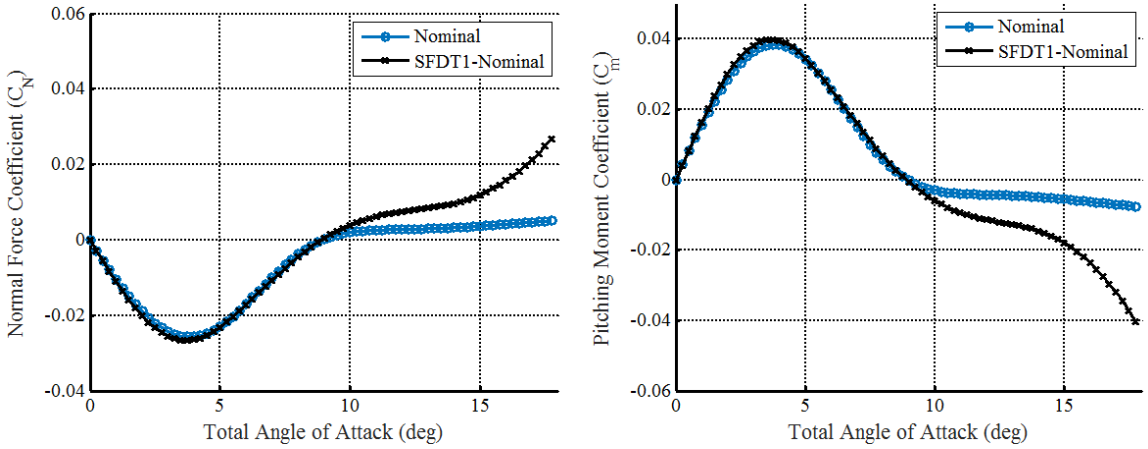

(a) Normal Force Coefficient

(b) Pitching Moment Coefficient at the moment reference point

Figure 6: A sample of the static aerodynamic data for the SFDT-2 Ringsail parachute and comparison with the SFDT-1 Disk-Sail data.

The lack of the strong restorative force and moment in the model meant that under the right environmental conditions, the parachute could have extremely large angles of attack and instability. However, the SFDT-2 parachutes are not believed to be unstable because the lack of the strong restorative force and moment was attributed to an artifact of the wind tunnel test matrix, where the maximum angle of attack was limited to 17.75 deg. It was instead believed by parachute experts that the SFDT-2 chute would trim at large angles of attack (something near 20 deg.).

For modeling the parachute in the flight dynamics simulation, the normal force and pitching moment coefficient data were augmented for angles of attack larger than 17.75 deg., so that a strong restorative force and moment similar to the ones seen in the SFDT-1 parachute occurred starting at 17.75 deg. One of the justifications for this change was that this augmentation did not affect the crucial inflation load predictions from the simulation, since those calculations were based on the unchanged drag-only data. Additionally, due to the dearth of information about large angle of attack behavior of supersonic Ringsail parachutes before the SFDT-2 flight, the static aerodynamic augmentation was believed to be reasonable by parachute experts and it was hoped that the SFDT-2 flight test data would be a good arbiter of that rationale.

Finally, another change made to the modeling of the supersonic Ringsail parachute was the parachute behavior in the event of a partial or full failure of the parachute. SFDT-1's Disk-Sail suffered a parachute failure and it was estimated that the remaining strands of the parachute provided drag equivalent to 2.5% of a full chute[9]. For range safety reasons and to aid recovery of flight articles, it was important to predict the splashdown footprint of the vehicle in the event of a chute failure. For SFDT-1, these predictions were based on no drag being produced by the parachute. The SFDT-1 experience, however, showed that a failed parachute still produces some drag, thus affecting the splashdown footprint prediction by several kilometers. For SFDT-2, a "streamer configuration" model was added to the simulation to produce a splashdown footprint prediction for a partial chute in addition to the splashdown footprints predicted by a nominal parachute behavior or a full failure of the chute (**Figure 7**). The drag coefficient of the streamer configuration was based on the post-flight assessment of the drag produced by the SFDT-1 chute

after failure[9]. This approach worked remarkably well for SFDT-2, ensuring efficient and successful recovery of the TV.

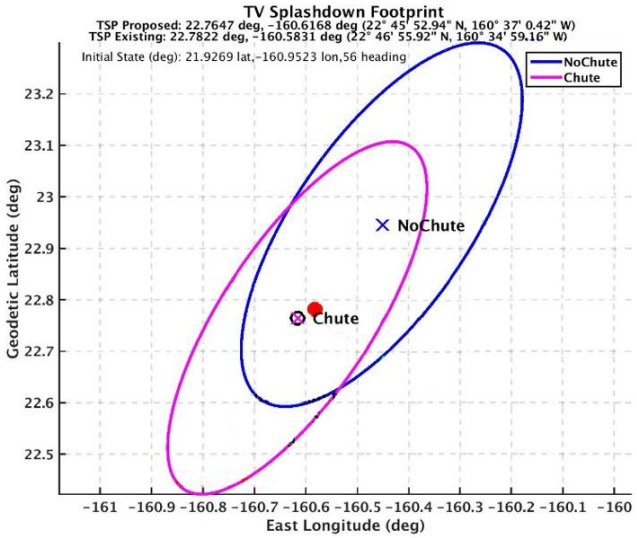

Figure 7: Sample splashdown footprint data for both nominal and chute failure scenarios.

Day-Of-Flight Atmospheric Modeling

During operations, a multi-body 6DOF simulation is used to help predict splashdown location and aid recovery efforts. This simulation differs somewhat from that used in flight dynamics analysis performed prior to flight, primarily in the initial state and the atmosphere model. Because the actual initial state is available during operations, it is no longer dispersed in Monte Carlo analyses as is done in pre-flight studies. Additionally, the GRAM atmosphere model used in pre-flight analyses is unnecessarily conservative when a current, local model is available, such as the Global Forecast System (GFS) modeling data or data from balloon tests. Temperature, density, east-west winds, and north-south winds are all modeled in the simulation.

For SFDT-1, a 24-hour GFS forecast was used as the atmosphere model in operations simulations. However, the variation on the predicted atmospheric data used in operational Monte Carlo analyses was derived from monthly GFS forecast data (i.e. climate variability). This was deemed an over conservative approach given the availability of actual radiosonde balloon data that could be compared with GFS 12 and 24 hour forecast data to provide a variation model.

GFS and balloon data sets were provided covering four years (2011-2014) for May 15 to July 15 at Lihue Airport. This data included both 12 and 24 hour GFS forecasts valid at two different times of the day. It was concluded that the GFS 12 and 24 hour forecast variations from actual are very similar, with no consistent significant advantage/improvement in using the 12 hour forecast rather than the 24 hour forecast. Additionally, no difference was noted in the forecast accuracy when accounting for the time of day the forecast was valid at, so the GFS forecast that was valid at the time closest to SFDT2 flight was used. No consistent bias was observed between the GFS forecast and actual data observed at the valid time of the forecast. Variability in temperature and density between GFS forecast and actual averaged 3% with wider variability between forecast and actual winds. Part of the wider wind variability could be attributed to the GFS data not accounting for small-scale variations like thunderstorms and the fact that balloon data is assumed to be a strictly vertical profile when in reality it is not. The forecast performance does vary with pressure level

and appears to show higher variability around certain pressure levels (i.e. ~15KPa and 75-80KPa). These pressure zones of greater variability appear to be reflections of the GFS forecast's ability to accurately model the location of upper level low pressure systems that are common in the area during the May to July timeframe. The atmospheric variations between forecast and truth appeared to be of Gaussian distribution and were binned into 16 different pressure levels which overlap with truth data, each with its own ±3σ bounds. This set of atmospheric variability was used in SFDT-2 operations for the simulation for best estimated trajectory and Monte Carlo splashdown footprint analyses.

Four different methods of applying the updated, pressure-dependent variation data were examined for comparison. **Figure 8** illustrates the basic differences in the methods while showing both the GFS and GRAM variation limits. Method 1 maintains the shape of the forecast profile and disperses the profile within the three sigma bounds the same for each parameter (i.e. a 1σ day in winds is a 1σ day in density at all pressure levels). This method of application was used in SFDT-1 operations.

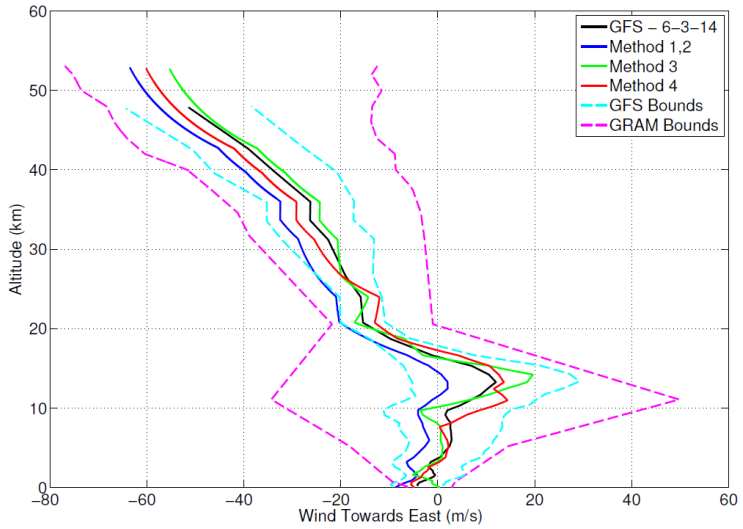

Figure 8: Sample dispersed wind profiles from the various application methods. GFS and GRAM bounds are also shown for reference. Methods 1 and 2 only differ between parameters, thus only one profile is shown to represent both as this is a single parameter plot of east-west winds

Method 2 is similar to the first except that it decouples the parameters. A dispersed profile will have the same variation across pressure levels, but the temperature dispersion can differ from the wind dispersions.

Method 3 further decouples the parameters by allowing different variation levels from one pressure bin to another (i.e. 1σ variation at 15K Pa and -2σ at 20K Pa). This method does not maintain the shape of the forecast profile and does allow a profile to go from one dispersed extreme to another between pressure levels.

Method 4 uses the balloon profile data described previously. There are approximately 600 of these profiles and one is selected at random for each dispersed run with this method. The difference between the random balloon profile at a given pressure level and GFS forecast at the same pressure level is the variability that is applied at that pressure level. Given a Monte Carlo set of 2000-8000 runs, each profile would be used multiple times.

A Monte Carlo analysis was run using each method and the splashdown footprints plotted for comparison in **Figure 9**. Red circles indicate distance from TV drop location in nautical miles SFDT-1 data (black) is plotted for reference and is below the Method 1 data (cyan) as the methods are the same. Decoupling the atmospheric parameters in Method 2 (blue) shows some minor difference. Method 3 (green) also decouples pressure levels and aligns with the balloon profiles of Method 4 (red).

The results from Method 3 coincide very well with the actual balloon data, without being limited to the 600 unique profiles delivered. For this reason, this method was selected for use during SFDT-2 operations. This method allows a more representative atmosphere dispersion set, rather than relying on unnecessarily conservative models.

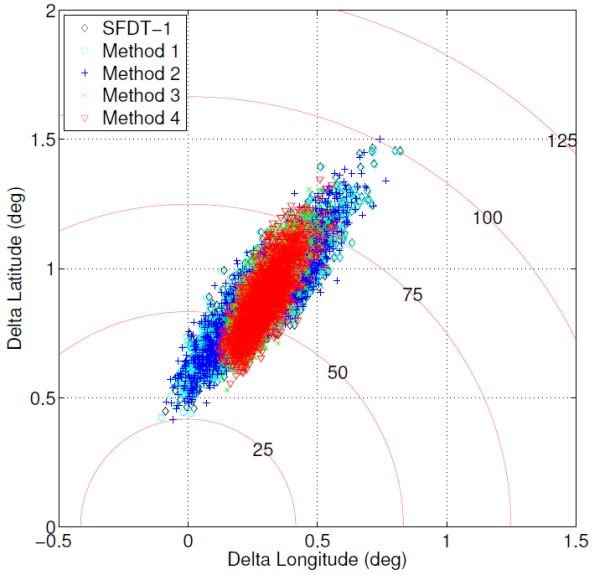

Figure 9: Splashdown footprints from the various GFS dispersion methods.

Flight Software Dynamic Event Triggering

Event triggering has also been updated to improve analysis capabilities for SFDT-2. During SFDT-1 analysis and operations, the velocity triggers for camera cover release and PDD deploy were static values. Dynamic triggering based on altitude at main motor burnout was employed for SFDT-2. A different polynomial curve fit was used for each trigger. **Figure 10** illustrates the polynomial fit used by the flight software and the corresponding Monte Carlo velocity and altitude data.

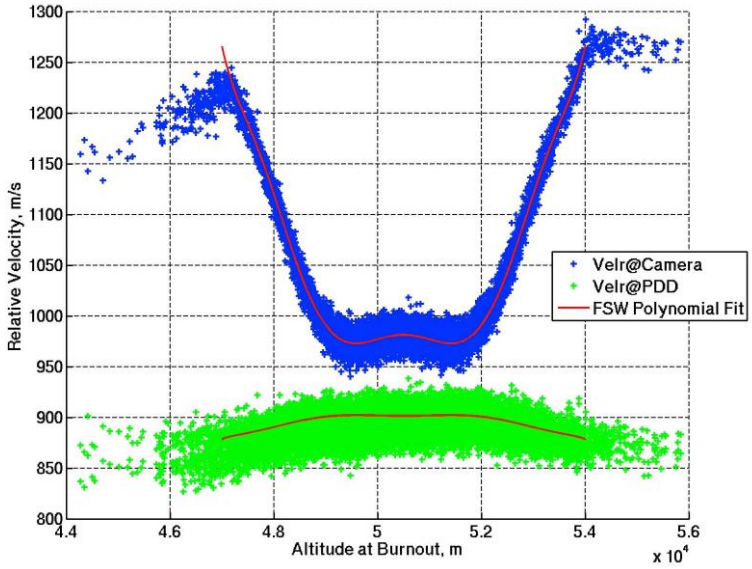

Figure 10: Dynamic triggering results and FSW polynomial fit.

With static event triggers, a single velocity is used to start an event, despite any other conditions. Dynamic triggering allows for the velocity of the trigger to vary with the altitude at main motor burnout. No-earlier-than (NET) and no-later-than (NLT) triggers are in place as backup triggers in the event that conditions are met outside an acceptable time window. The tails in the figure that vary from the polynomial fit are cases where the NET or NLT backup time triggers were used. The dynamic triggering update allowed for improved event conditions at SIAD deploy (via camera cover trigger) and PDD deploy by correlating to the altitude at main motor burnout.

CONCLUSION

The LDSD project has completed two flights of its SFDT vehicle. The POST2 simulation tool was heavily used in pre-flight and operations analysis for both SFDT-1 and SFDT-2. Many valuable insights were gathered from reconstruction work for SFDT-1 and specific models in POST2 were identified for updates and improvements in preparation for SFDT-2 which launched in June 2015.

Various model updates have been described here along with their impact on analysis and operations. The main motor thrust and dispersion modeling dramatically improved the ability of POST2 to capture as-flown thrust profiles. Test vehicle aerodynamics were updated to more realistically capture behavior at low Mach values which heavily affected downstream events. The PDD, which was previously ignored in simulation once released, was modeled aerodynamically during free-flight and tracked to splashdown, allowing for successful recovery of the flight hardware. The parachute aerodynamics were updated to reflect the design change to an SSRS and allow simulation of a low drag, streamer scenario, again aiding in recovery efforts. Updates were applied to the day-of-flight atmospheric modeling to more accurately match local balloon test data. Finally, dynamic event triggering was implemented to improve the timing of critical events to achieve desired conditions.

All of these updates made for a more robust set of simulations to be used for pre-flight analysis and operations, including recovery efforts. While a discussion of reconstruction efforts is reserved for another document[10], the capability added with these updates improved and added insight to those efforts as well.

[1] Clark, I., Adler,A., and Rivellini, T., "Development and Testing of a New Family of Low Density Supersonic Decelerators." AIAA 2013-1252, 22nd AIAA Aerodynamic Decelerator Systems Conference, March 2013, Daytona Beach, FL.
[2] B.T. Cook et al., "High Altitude Supersonic Decelerator Test Vehicle." AIAA 2013-1353, 22nd AIAA Aerodynamic Decelerator Systems Conference, March 2013, Daytona Beach, FL.
[3] Bauer, G.L., Cornick, D.E., and Stevenson, R., "Capabilities and Applications of the Program to Optimize Simulated Trajectories (POST)." NASA CR-2770, February 1977.
[4] Bowes, A., Davis, J., Dutta, S., Striepe, S., Ivanov, M., Powell, R., and White, J., "LDSD POST2 Simulation and SFDT-1 Pre-Flight Launch Operations Analyses," AAS Paper 15-232, January 2015.
[5] Dutta, S., Bowes, A., Striepe, S., Davis, J., Queen, E., Blood, E., and Ivanov, M., "Supersonic Flight Dynamics Test 1 - Post-Flight Assessment of Simulation Performance," AAS Paper 15-219, January 2015.
[6] P. Kutty et al., "Supersonic Flight Dynamics Test One: Trajectory, Atmosphere, and Aerodynamics Reconstruction," AAS 15-224, AAS/AIAA Space Flight Mechanics Conference, 11-15 January 2015, Williamsburg, VA.
[7] J. Van Norman, A. Dyakonov, M. Schoenenberger, J. Davis, S. Muppidi, C. Tang, D. Bose, B. Mobley, and I. Clark, "Aerodynamic Models for the Low Density Supersonic Decelerator (LDSD) Test Vehicles," Paper Submitted, AIAA Aviation 2016 Conference, Washington, DC, 2016.
[8] C. O'Farrell, E. J. Brandeau, C. Tanner, J. Gallon, S. Muppidi, and I. Clark, "Reconstructed Parachute System Performance During the Second LDSD Supersonic Flight Dynamics Test," Paper Submitted, AIAA Atmospheric Flight Mechanics Conference, Washington, DC, 2016
[9] I. Clark and E. Blood, "Low-Density Supersonic Decelerator (LDSD) Supersonic Flight Dynamics Test-1 (SFDT-1) Post-Test Report," JPL Document D-81940, *NASA Jet Propulsion Laboratory*, Pasadena, CA, 2015
[10] S. Dutta, A.L. Bowes, J.P. White, S.A. Striepe, E. M. Queen, C. O'Farrell, and M.C. Ivanov, "Post-flight assessment of low density supersonic decelerator flight dynamics test 2 simulation," AAS 16-222, AAS/AIAA Space Flight Mechanics Conference, Napa, CA, 2016